Environmental Science
Water Research & Technology

ROYAL SOCIETY OF CHEMISTRY

PAPER

View Article Online
View Journal | View Issue

Cite this: *Environ. Sci.: Water Res. Technol.*, 2024, **10**, 2765

Shallow Shell SSTA63 resin: a rapid approach to remediation of hazardous nitrate

Elif Çendik,[a] Mügenur Saygı,[a] Yaşar Kemal Recepoğlu [b] and Özgür Arar *[a]

Received 11th July 2024,
Accepted 26th August 2024

DOI: 10.1039/d4ew00584h

rsc.li/es-water

This study examines the potential of Purolite Shallow Shell™ SSTA63 anion exchange resin for mitigating nitrate ion (NO_3^-) contamination in aqueous environments. Through systematic experimentation, including dosage optimization, pH dependency, kinetic and desorption studies, we investigate the sorption behavior and practical applications of the resin. Results indicate that the resin effectively removes NO_3^- ions, with maximum efficiency achieved within 10 minutes. When 0.025 g of resin was used, 75% of NO_3^- was removed, whereas with 0.05 g, 89% was removed, and with 0.1 g of resin, 95% was removed. At pH 1, approximately 50% of NO_3^- ions were removed, with removal efficiency reaching 97% between pH 4 and 10. Sorption isotherms affirm the suitability of the Langmuir model for the current investigation. The monolayer maximum sorption capacity (q_{max}) value was found to be 53.65 mg g^{-1}. The resin demonstrates robust desorption capabilities using 0.1 M hydrochloric acid (HCl), effectively desorbing NO_3^- above 99%, indicating easy NO_3^- desorption and resin regeneration. The presence of coexisting ions such as chloride (Cl^-), sulfate (SO_4^{2-}), and phosphate (PO_4^{3-}) showed a minimal impact on NO_3^- removal in individual binary mixtures, with efficiencies exceeding 93%, suggesting a strong selectivity of the resin towards NO_3^-. Purolite SSTA63 anion exchange resin exhibited a high affinity for NO_3^- ions, even over other competing ions, despite the general trend of ion exchange resins to favor ions with a higher atomic number and valence. Overall, this resin presents a promising solution for NO_3^- removal, with implications for water treatment and environmental remediation.

Water impact

Our study highlights Purolite Shallow Shell™ SSTA63 resin as a highly effective solution for mitigating nitrate ion (NO_3^-) contamination in water. Utilizing advanced anion technology that strategically deactivates the gel bead center, the resin shows rapid and efficient removal within 10 minutes and robust regeneration capabilities with hydrochloric acid. Minimal interference from coexisting ions emphasizes its reliability in diverse environmental conditions, suggesting broad applicability in water treatment and environmental remediation efforts.

1. Introduction

Water, a critical component of Earth's hydrological cycle, is increasingly compromised by anthropogenic activities. Population growth, industrial expansion, and elevated consumption patterns have exacerbated water scarcity and pollution. In aquatic environments, emerging contaminants, including chemical residues, microbial pathogens, and heavy metals, pose significant risks to ecosystems and human health. Consequently, developing and implementing robust water treatment technologies are imperative to safeguard water quality and ensure sustainable resource management.[1–4] Nitrate (NO_3^-) pollution in water is a significant global concern, driven by agricultural runoff, industrial discharges, and improper waste management, posing threats to the environment and human health.[5,6] Studies indicate that NO_3^- is among the most prevalent compounds found in water.[7] NO_3^- is a salt ion of nitric acid (HNO_3).[8] A healthy individual typically consumes 75 to 100 mg of NO_3^- daily, but regular vegetable consumption can raise this intake to 250 mg per day. To balance NO_3^- levels, a varied diet is essential.[9–11] The NO_3^- level obtained from deep water sources may vary. When comparing the NO_3^- content per liter of surface water sources with that of well water, it is observed that surface water sources generally contain 80% less NO_3^-. This is a significant difference; adjusting water consumption according to NO_3^- intake would be beneficial.[12] According to WHO data, 80% of diseases in developing countries are linked to drinking water, making it one of the top three hazardous substances. Daily water pollution with toxic and carcinogenic substances and dwindling clean water sources have driven the development of

[a] *Department of Chemistry, Faculty of Science, Ege University, Bornova, Izmir 35040, Türkiye. E-mail: ozgur.arar@ege.edu.tr*
[b] *Department of Chemical Engineering, Faculty of Engineering, Izmir Institute of Technology, Urla, Izmir 35430, Türkiye*

wastewater recycling processes.[13] NO_3^- contamination in waterways mainly stems from using nitrogen-based fertilizers in agriculture. Ammonium, sodium, potassium, and calcium salts are the primary NO_3^- fertilizers, with millions of kilograms produced annually. Although vital for crop yields and food security, these fertilizers often leave excess nitrogen leaching into groundwater and surface waters, worsening NO_3^- pollution.[14–17] Furthermore, industrial processes and urban runoff contribute to NO_3^- pollution, featuring the multifaceted nature of the problem.[18,19] For example, nitrates are oxidizing agents in explosives, facilitating the rapid oxidation of carbon compounds and releasing gases in large volumes.[20–22] Sodium nitrate is used to remove air bubbles from molten glass and certain ceramics.[23] Mixtures of molten nitrate salts are used to harden some metals.[24] The ramifications of NO_3^- pollution extend far beyond mere environmental degradation. NO_3^- toxicity can arise through the enterohepatic metabolism of NO_3^- that harms health, mainly when converted into nitrite (NO_2^-).[25–28] Toxicosis can be defined as a form of toxin poisoning. When ingested *via* contaminated drinking water sources, NO_3^- poses significant health risks, particularly in vulnerable populations such as infants and pregnant women.[29–31] Excessive intake of the carcinogenic nitrate can lead to stomach cancer.[32,33] NO_3^- cannot carry oxygen as it oxidizes the iron atoms in hemoglobin. This process can result in a general lack of oxygen in organ tissues and a dangerous condition known as methemoglobinemia.[34–36] Although NO_3^- can be converted into ammonia, organisms may slowly perish due to oxygen deprivation if an excessive amount cannot be converted.[37] Moreover, elevated NO_3^- concentrations can lead to harmful algal blooms, which not only disrupt aquatic ecosystems but also release toxins harmful to aquatic life and human health.[38]

Despite these formidable challenges, concerted efforts to develop effective NO_3^- removal strategies have become imperative. Traditional approaches such as ion exchange,[39] adsorption,[40] and biological denitrification[41] have long been employed to mitigate NO_3^- pollution. Some emerging technologies, including membrane filtration,[42,43] electrochemical treatment,[44–46] and phytoremediation,[47,48] also offer efficient and sustainable NO_3^- removal. Among them, the ion exchange method has superior properties. Exceptional selectivity enables targeted removal or exchange of specific ions from solutions, making it invaluable in water purification, metal recovery, and pharmaceutical industries.[49,50] In addition, ion exchange resins exhibit high capacity and efficiency, ensuring optimal ion removal with minimal resin usage. Their robust physical and chemical stability ensures prolonged lifespan and reliability even under harsh conditions. Moreover, these resins offer versatility, accommodating diverse pH levels and temperatures and enhancing their suitability for various processes.[51] A wide range of sorbents, from traditional materials to advanced nanomaterials, have been investigated to remove various pollutants. As research progresses, there is an increasing need for more efficient sorbents capable of rapid and effective pollutant removal. There is a significant demand for materials across various industries due to their ability to precisely alter their physical properties in response to environmental stimuli, including temperature fluctuations, mechanical stress, magnetic fields, chemical exposure, electrical currents, pH variations, and hydrostatic pressure.[52,53] Beyond, as ion exchange materials are being developed, shallow shell technology (SST) represents a significant advancement in ion exchange resin design, offering numerous advantages over traditional resin structures. This innovative approach involves engineering resin particles with a thin, highly accessible outer layer, which enhances mass transfer kinetics and efficiency. One notable advantage of SST is its superior accessibility to active sites, facilitating faster ion exchange kinetics and improving overall process performance. On the other hand, the reduced diffusion path length within the shallow shell structure enhances the capacity of resin for ion exchange, leading to higher throughput and increased productivity (Fig. 1). Their enhanced resistance to fouling and chemical degradation further proves their suitability for demanding industrial applications. SST in ion exchange resins offers unmatched efficiency, capacity, and durability, making it a preferred choice for diverse separation and purification processes.[54]

This work examines the efficacy of Purolite Shallow Shell™ SSTA63 anion exchange resin for removing NO_3^- from aqueous solutions for the first time in the literature. Through systematic experimentation, the interplay between resin dosage, pH levels, and the presence of coexisting ions is investigated, aiming to elucidate optimal conditions for enhancing removal efficiency while minimizing resin utilization. The thermodynamic aspects governing the interaction between the resin and NO_3^- ions are explored. By unraveling the underlying mechanisms driving NO_3^- removal by the Purolite resin, contributions to advancements in water quality management and environmental remediation efforts are sought. This study introduces an innovative approach to NO_3^- removal by employing a resin enhanced by the SST as a key material. The application of this ion exchange resin further distinguishes this work, allowing for unprecedented insights into reduced diffusion path length. Integrating ion exchange resin with SST ensures a comprehensive evaluation of removing NO_3^-, setting

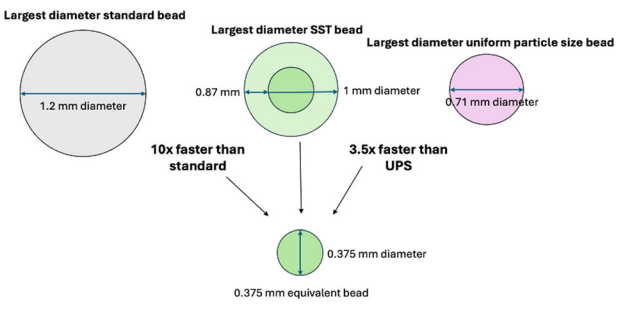

Fig. 1 Diffusion path comparison of different resin bead types (adapted from the Purolite SST ion exchange resin catalog).

Table 1 Typical physical and chemical properties of Purolite Shallow Shell™ SSTA63 anion exchange resin

Polymer structure	Gel polystyrene crosslinked DVB
Appearance	Spherical beads
Functional group	Type II quaternary ammonium
Ionic form	Cl^- form
Dry weight capacity (min.)	2.6 eq. kg^{-1} (Cl^- form)
Moisture retention	37–45% (Cl^- form)
Particle size range	300–1200 μm
Specific gravity	1.12
Temperature limit	35 °C (95 °F)

this research apart from existing studies in the field. The combination of this advanced material and method not only enhances the accuracy of the findings but also offers a scalable solution for NO_3^- remediation.

2. Experimental

2.1. Materials

Sodium nitrate ($NaNO_3$), sodium chloride (NaCl), and sodium hydroxide (NaOH) were procured from Merck with a stated purity of 99%. Hydrochloric acid (HCl) of 37% concentration was obtained from Carlo Erba. These chemicals were selected for their high purity to ensure the integrity of the experimental procedures and the reliability of the results. In addition, Purolite Shallow Shell™ SSTA63 anion exchange resin, acquired from Purolite, was employed as the sorbent in the study. This resin was chosen for its documented properties in the targeted ion exchange processes efficiency, as given in Table 1.

2.2. Conditioning of Purolite SSTA63 anion exchange resin

Before using in sorption/desorption studies, conditioning the Purolite SSTA63 anion exchange resin was performed as follows: the wet resin (50 mL) was transferred into a plastic container, and 100 mL of a 2.0 M NaCl aqueous solution was added. The mixture was agitated at 250 rpm for 5 h using a shaker. Subsequently, the resins were filtered and washed with distilled water until the conductivity of the washing water approached that of pure water. The conditioned resin was then dried in an oven at 35 °C until reaching a constant weight, after which it was utilized in the experiments.

2.3. Sorption/desorption experiments of NO_3^- using Purolite SSTA63 anion exchange resin

To determine the optimum resin amount, conditioned and dried resins were weighed at 0.025, 0.05, 0.1, 0.2, and 0.3 g and placed into plastic bottles containing 25 mL of a 100 mg L^{-1} NO_3^- solution (pH 6), and they were agitated in a shaker for 24 h. The optimum operating pH was determined by the contact of the optimum amount of resin with 25.0 mL of 100 mg L^{-1} NO_3^- solutions prepared at different pH levels (pH: 1, 2, 4, 6, 8, and 10) using solutions of HCl and NaOH for 24 h. The effect of contact time was investigated through kinetic tests where 4.0 g of SSTA63 resin was added to a 1000 mL solution containing 100 mg L^{-1} NO_3^- and mixed at 25 °C and 300 rpm. Samples of 10.0 mL were collected from the solutions at specified time intervals. For sorption isotherm studies, the resin in the optimum quantity was equilibrated with 25 mL solutions containing 50, 100, 200, 400, and 600 mg L^{-1} concentrations of NO_3^- at 30 °C for 24 h. For thermodynamic studies, the optimum quantity of resin was agitated for 60 min at different temperatures (15, 20, 30 °C) with 25 mL taken from a solution containing 200 mg L^{-1} NO_3^-.

After equilibrating, the resins were separated by filtration, and the initial and remaining NO_3^- concentrations in the solution were measured. The percentage removal of NO_3^- and the sorption capacity of the sorbent were calculated by the following equations (eqn (1) and (2)):

$$\text{Removal of } NO_3^- \ (\%) = \frac{C_0 - C_e}{C_0} \times 100 \quad (1)$$

$$q_e = \frac{(C_0 - C_e)V}{m} \quad (2)$$

where C_0 and C_e are the initial and equilibrium concentrations (mg L^{-1}), respectively. q_e is the sorption capacity at equilibrium (mg g^{-1}), V is the solution volume (L), and m is the dry weight of the sorbent.

The desorption process was conducted in two steps. In the first step, NO_3^- ions were loaded onto the SSTA63 resin. 1 g of dry resin was weighed, and 100 mL of a 1000 mg L^{-1} NO_3^- solution was added. The mixture was agitated in a shaker for 3 h, and then the resin was separated by filtration, washed with distilled water, and dried in an oven until a constant weight was achieved. The remaining NO_3^- concentration in the filtrate was measured to calculate the amount of NO_3^- retained by the resin. In the second step of the study, the process of reclaiming the NO_3^- ions retained in the resin was performed. 0.025 g of NO_3^--loaded dry resin was weighed and agitated for 3 h with 25 mL of HCl solution at different concentrations (0.1, 0.5, 1.0, and 2.0 M). After filtration, the concentration of NO_3^- transferred to the solution was measured to calculate the desorption efficiency for each concentration using the formula provided below (eqn (3)):

$$\text{Desorption efficiency } (\%) = \frac{\text{The amount of } NO_3^- \text{ desorbed from the resin}}{\text{The amount of } NO_3^- \text{ loaded onto the resin}} \times 100 \quad (3)$$

The selectivity of the resin towards NO_3^- in the presence of Cl^-, SO_4^{2-} and PO_4^{3-} anions was investigated by contacting binary mixtures (25 mL) containing 100 mg L^{-1} of each NO_3^-, Cl^-, SO_4^{2-} and PO_4^{3-} and the optimum sorbent amount for 1 h separately.

The sorption/desorption experiments (except kinetic investigation) were performed in two parallel experiments, and the results were averaged; the difference between them was 4% or less, so 4% error bars have been added to the relevant figures.

2.4. Determination of NO_3^- concentrations

NO_3^- analyses were conducted spectrophotometrically at a wavelength of 200 nm using a quartz cuvette with the assistance of an Agilent Cary 60 UV-vis spectrophotometer instrument.

3. Results and discussion

3.1. The effect of resin dose on NO_3^- removal

The resin dose plays an important role in the removal of NO_3^- ions from water. Experimental observations in Fig. 2 indicate a notable relationship between the amount of resin used and the efficiency of NO_3^- removal. As demonstrated in our study, as the amount of resin increased, the removal rate of NO_3^- increased and eventually reached equilibrium. When 0.025 g of resin was used, 75% of NO_3^- was removed, whereas with 0.05 g, 89% was removed, and with 0.1 g of resin, 95% was removed. Since the removal rate did not change with higher resin usage, 0.1 g of resin was determined as the optimum amount. Specifically, with an increase in resin quantity, the number of functional groups utilized for NO_3^- sorption increased, thereby enhancing the removal rate of NO_3^-. However, it is noteworthy that after reaching a certain threshold, further increments in resin dose did not yield significant improvements in removal rates, suggesting the attainment of equilibrium conditions.

3.2. The effect of pH on NO_3^- removal

As illustrated in Fig. 3, the removal efficiency of NO_3^- ions using Purolite SSTA63 resin exhibits variations with changes in solution pH. At pH 1, approximately 50% of NO_3^- ions were removed. Upon increasing the solution pH from 1 to 3, the removal efficiency rose from 50% to 89%, reaching a value of 97% between pH 4 and 10. The diminished removal efficiency observed at lower pH values can be attributed to interference from Cl^- ions introduced into the environment by adding HCl solution for pH adjustment. As the pH increases, the introduction of Cl^- ions into the environment decreases, consequently reducing the interference effect and increasing NO_3^- removal efficiency.

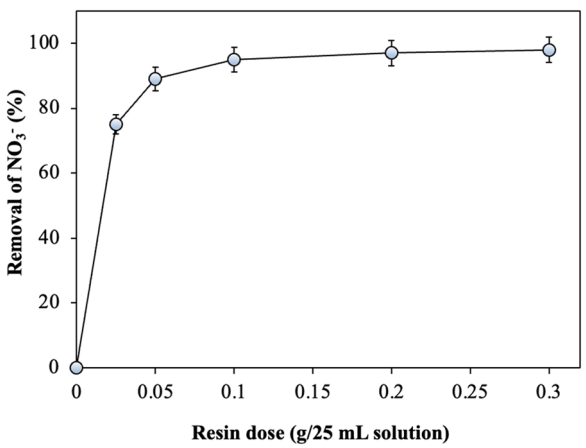

Fig. 2 The effect of resin dose on the removal efficiency of NO_3^- from water by Purolite SSTA63 anion exchange resin (C_0 = 100 mg L^{-1}; pH = 6; T = 25 °C; contact time = 24 h).

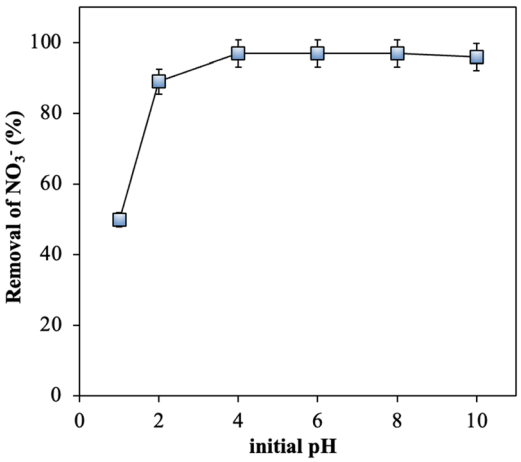

Fig. 3 The effect of pH on the removal efficiency of NO_3^- from water by Purolite SSTA63 anion exchange resin (C_0 = 100 mg L^{-1}; resin dose = 0.1 g/25 mL solution; T = 25 °C; contact time = 24 h).

Purolite SSTA63 resin operates *via* an anion exchange mechanism, wherein NO_3^- in the water is exchanged for other anions on the resin. The resin contains positively charged functional groups that attract and exchange anions in the surrounding solution. The resin is typically in its Cl^- form at low pH (acidic conditions). The resin has a high affinity for NO_3^- ions in the water in this form. The exchange process involves Cl^- ions being released from the resin into the solution while NO_3^- ions are captured by the resin.

$$\text{Resin-Cl}^- + \text{NO}_3^- \rightleftharpoons \text{Resin-NO}_3^- + \text{Cl}^-$$

3.3. The effect of contact time on NO_3^- removal and sorption kinetics

The sorption of NO_3^- on Purolite SSTA63 anion exchange resin over varying contact times was examined at 25 °C. Analysis revealed swift NO_3^- sorption within the initial minutes, followed by a decrease until reaching equilibrium, as illustrated in Fig. 4(a). The initial rapid sorption can be ascribed to the abundant available binding sites on the resin surface. Subsequently, the sorption rate decelerated as the active sites became saturated. Maximum removal of NO_3^- was achieved within the first 5 min of contact time, and equilibrium sorption was attained after 10 min.

The kinetics of NO_3^- sorption on Purolite SSTA63 anion exchange resin was assessed utilizing pseudo-first-order (PFO) and pseudo-second-order (PSO) kinetic models.[55] Fig. 4(b) and (c) show the linear plots of PFO and PSO, respectively. Detailed rate equations and associated values

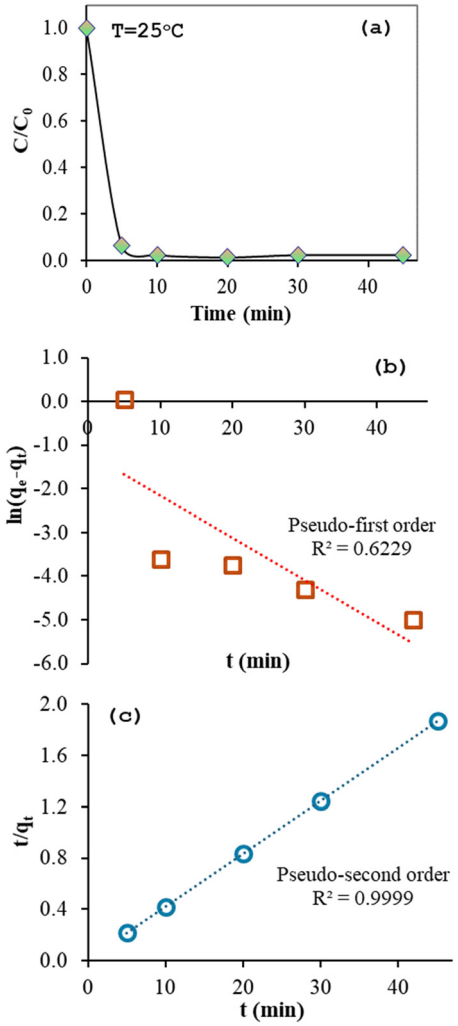

Fig. 4 (a) The effect of contact time on NO_3^- sorption onto Purolite SSTA63 resin and sorption kinetics fitting plots by (b) pseudo-first order model, (c) pseudo-second order model.

are presented in Table 2. The results obtained from the PSO model demonstrated good agreement with the experimental data, thereby providing a favorable explanation for NO_3^- sorption on the resin. The correlation coefficient (R^2) for the PSO model surpassed those for the PFO model, and the calculated $q_{e,cal}$ (24.15 mg g^{-1}) values from the PSO model closely approximated the experimental $q_{e,exp}$ (24.05 mg g^{-1}) values compared to the calculated $q_{e,cal}$ (0.30 mg g^{-1}) values from the PFO.

3.4. Sorption isotherms

Sorption equilibrium is typically characterized by an isotherm equation, which describes the affinity and surface properties of the sorbent under specific pH and temperature conditions. These equations establish the relationship between the quantity of sorbate adhered to the sorbent and the concentration of dissolved sorbate in the liquid phase at equilibrium, referred to as sorption isotherms. The sorption isotherms aid in characterizing the pollutant removal process using sorbents, shedding light on physical/chemical phenomena, favorable sorption, sorption energy, and the distinction between single-layer and multilayer sorption scenarios.[56] These equations, often used to describe experimental isotherms, were developed by Freundlich, Langmuir, Dubinin–Radushkevich (D–R), and Temkin.

Fig. 5 illustrates the fitting of isotherm models alongside experimental data, providing insights into the sorption behavior of NO_3^- onto Purolite SSTA63 resin. Table 3 represents the isotherm models with their associated parameters and values. The experimental dataset exhibited a strong fit with the Langmuir model. The plots depicting $1/q_e$ *versus* $1/C_e$ for the NO_3^- sorption onto the resin displayed linear relationships with high correlation coefficients (>0.99), affirming the suitability of the Langmuir model for the current investigation. The monolayer maximum sorption capacity (q_{max}) and Langmuir constant (K_L) values were found to be 53.65 mg g^{-1} and 0.0688, respectively. The q_{max} value obtained from the Langmuir isotherm closely matched the experimental value at the specified temperature. These findings suggest that NO_3^- sorption is in a monolayer coverage configuration. To assess the favorability of sorption, the influence of sorption isotherm shape has been investigated,[55] focusing on the dimensionless constant 'R_L', also known as the separation factor or equilibrium parameter. The calculation of 'R_L' is carried out using the equation provided below (eqn (4)):

Table 2 Linear rate equations and their associated values for the model and fitting parameters for NO_3^- sorption on Purolite SSTA63 anion exchange resin

Kinetic model	Linear equation[a]	Parameters	Values
Pseudo-first order	$\ln(q_e - q_t) = \ln q_e - k_1 t$	k_1	0.097
		$q_{e,cal}$	0.300
		$q_{e,exp}$	24.050
		R^2	0.623
Pseudo-second order	$\frac{t}{q_t} = \frac{1}{k_2 q_e^2} + \frac{1}{q_e} t$	k_2	0.301
		$q_{e,cal}$	24.150
		$q_{e,exp}$	24.050
		R^2	0.999

[a] q_t: instantaneous sorption capacity (mg g^{-1}), k_1: sorption rate constant of PFO model (min^{-1}), k_2: sorption rate constant of PSO (g mg^{-1} min^{-1}).

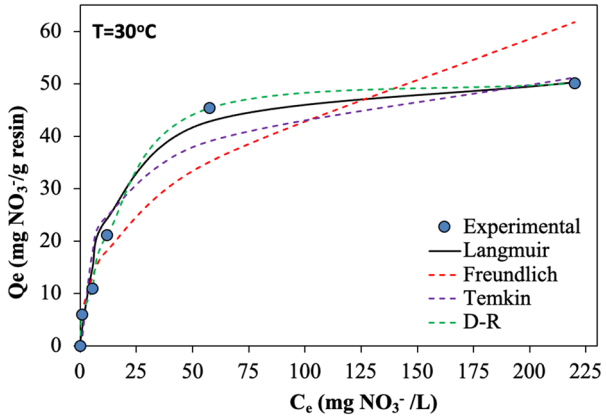

Fig. 5 Comparison of NO_3^- sorption isotherm fitting and experimental data for Purolite SSTA63.

Table 3 Isotherms models with associated parameters and values for sorption of NO_3^- on Purolite SSTA63 anion exchange resin

Isotherm model	Nonlinear equations[a]	Parameters	Values
Langmuir	$q_e = \frac{q_{max} K_L C_e}{1 + K_L C_e}$	q_{max} (mg g^{-1})	53.65
		K_L (L mg^{-1})	0.0688
		R^2	0.9962
Freundlich	$q_e = K_F C_e^{1/n}$	K_F	6.3777
		n	2.3751
		R^2	0.9511
Temkin	$q_e = B \ln(A_T C_e)$	b_T (J mol^{-1})	272.24
	$B = RT/b_T$	A_T (L mol^{-1})	1.26
		R^2	0.9244
D–R	$q_e = q_{max} \exp(-\beta\varepsilon^2)$	β (mol^2 kJ^{-2})	0.0045
	$\varepsilon = RT \ln\left(1 + \frac{1}{C_e}\right)$	E (kJ mol^{-1})	10.54
	$E = \frac{1}{\sqrt{2\beta}}$	q_{max} (mg g^{-1})	51.68
		R^2	0.9622

[a] K_L: Langmuir isotherm constant (L mg^{-1}); K_F and n: Freundlich isotherm constants; B: Temkin isotherm constant related to the heat of sorption, A_T: equilibrium binding constant (L mg^{-1}), R: universal gas constant (8.314 J mol^{-1} K^{-1}), T: absolute temperature (K); β: adsorption energy constant (mol^2 kJ^{-2}), E: mean free energy (kJ mol^{-1}).

$$R_L = \frac{1}{1 + K_L C_0} \quad (4)$$

The obtained R_L values, ranging between 0 and 1, confirm the favorable nature of the sorption isotherm for all initial concentrations. This conclusion is also strongly supported by the finding concerning the $1/n$ value obtained from the Freundlich isotherm. The Freundlich constants, represented by the parameters n and K_F, were calculated as 2.3751 and 6.3777, respectively. Despite relatively less fitting experimental data (R^2 = 0.9511) than Langmuir isotherm, these values indicate that NO_3^- is favorably sorbed by the resin. Temkin proposed that the heat of sorption of all molecules within the sorbent layer decreases linearly with coverage, thereby governing the interactions between the sorbate and sorbent. The positive b_T value (+272.24 J mol^{-1}) obtained from the Temkin model indicated an exothermic process of NO_3^- suggesting the presence of electrostatic interactions.[57] In D–R isotherms, the nature of sorption can be discerned through the calculated mean adsorption energy (E). The process will likely be chemical if the E values surpass 8–16 kJ mol^{-1}. Conversely, lower E values suggest physical adsorption.[58] In this study, the calculated experimental value of E was found to be 10.54 kJ mol^{-1}, indicating the ion exchange of NO_3^- ions with resin functional group. However, a relatively low correlation coefficient may lead to a deviation in numerical values as the nature of the sorption was found to be a physical sorption in thermodynamic analysis, which was discussed later in detail.

The sorption capacities of our applied sorbent that is Purolite SSTA63 anion exchange resin and several others recently utilized, mostly featuring commercially available anion exchange resins such as Purolite A 520E, Amberlite IRA 400, D417, Dowex 21K XLT *etc.* are presented in Table 4. Notably, the Purolite SSTA63 resin, utilized in this study, demonstrates distinct kinetics and isotherm models in the removal of NO_3^- compared to other reported sorbents, thereby highlighting its promising efficacy in NO_3^- removal.

3.5. Sorption thermodynamics

The nature and thermodynamic feasibility of the sorption process were assessed by analyzing the thermodynamic constants, including the standard free energy ($\Delta G°$, kJ mol^{-1}), standard enthalpy ($\Delta H°$, kJ mol^{-1}), and standard entropy ($\Delta S°$, kJ mol^{-1} K^{-1}), using eqn (5)–(8):

$$\Delta G° = \Delta H° - T\Delta S° \quad (5)$$

$$\Delta G° = -RT \ln K_D \quad (6)$$

$$\ln K_D = \frac{\Delta S°}{R} - \frac{\Delta H°}{RT} \quad (7)$$

$$K_D = q_e/C_e \quad (8)$$

where K_D is the equilibrium distribution constant.

Fig. 6 is the plot of $\ln K_D$ *vs.* $1/T$ to estimate the $\Delta H°$ and $\Delta S°$ for sorption of NO_3^- using Purolite SSTA63 resin from the slope and intercept, respectively. The summarized values of the aforementioned parameters are presented in Table 5. The sorption process exhibits spontaneity, as evidenced by the negative $\Delta G°$ value at all studied temperatures with increasing magnitudes as temperature also increased. Also, based on magnitude, $\Delta G°$ typically ranges from 0 to −20 kJ mol^{-1} for physical sorption and −80 to −400 kJ mol^{-1} for chemisorption.[68] Hence, the mechanism of NO_3^- sorption on resin relies on $\Delta G°$ values falling within the range of 0 to −20 kJ mol^{-1}, indicating physical sorption. On the other hand, the negative $\Delta H°$ value (−4.77 kJ mol^{-1}) indicates an exothermic interaction between NO_3^- and the resin. Meanwhile, the exothermic nature of the

Table 4 A comparative analysis of the studied sorbent (Purolite SSTA63 anion exchange resin) and various other sorbents for NO_3^- removal

Sorbent	Maximum sorption capacity (mg g^{-1})	Equilibrium constant[a]	Rate constant[b]	Ref.
Purolite A 520E	81.97	0.400^{L}	N.A.	59
Amberlite IRA 400	50.76	0.035^{L}	0.030^{PSO}	60
NDP-2	174.20	0.052^{L}	0.056^{PFO}	61
A 300	147.21	0.035^{L}	0.045^{PFO}	
D201	173.80	0.037^{L}	0.044^{PFO}	
D417 resin	23.46	8.200^{F}	0.0276^{PSO}	62
PS-WSR	43.88	0.042^{L}	0.036^{PSO}	63
PS-CSR	33.35	0.040^{L}	0.050^{PSO}	
LS-WSR	50.24	0.048^{L}	0.052^{PSO}	
LS-CSR	39.15	0.032^{L}	0.034^{PSO}	
ALR-AE resin	44.61	0.045^{L}	N.A.	64
Dowex 21K XLT	27.60	5.690^{F}	0.0033^{PSO}	65
Dowex 21K XLT-Fe doped	75.30	4.340^{F}	0.0077^{PSO}	
MFQ resin	124.10	4.644^{F}	0.025^{PSO}	66
PAN-PEI-5C	31.32	0.0600^{L}	0.119^{PSO}	67
Purolite SSTA63	53.65	0.0688^{L}	0.301^{PSO}	This work

[a] L: Langmuir; F: Freundlich. [b] PFO: pseudo-first order; PSO: pseudo-second order.

sorption process can be justified by the sorption capacities decreasing from 24.05 mg g^{-1} to 21.08 mg g^{-1} as the temperature increased from 25 to 30 °C under the same conditions. Given that the $\Delta H°$ value obtained in this study falls below 40 kJ mol^{-1}, it also suggests that physical adsorption predominates during the sorption process. This suggests that weak physical electrostatic and van der Waals interactions, rather than chemical bonds, are responsible for binding the NO_3^- ions to the functionally vacant sites of the resin.[69] Furthermore, the positive $\Delta S°$ value (+1.08 J mol^{-1} K^{-1}) indicates the affinity of the sorbent for NO_3^- as randomness increased in the sorption process.

3.6. Desorption of NO_3^- and selectivity studies

NO_3^- desorption experiments were conducted to recover and reuse the sorbent. The rationale behind this approach is to desorb the NO_3^- ions, initially retained from larger contaminated water volumes, to obtain concentrated solutions in smaller volumes. Consequently, both the resin and the NO_3^- can be recycled, facilitating sustainable utilization of resources.[70] Fig. 7(a) shows the desorption efficiencies for NO_3^- at different HCl concentrations varying from 0.1 M to 2.0 M. Even the lowest molarity of 0.1 M HCl could effectively desorbed NO_3^- above 99%, indicating easy NO_3^- desorption and resin regeneration.

Fig. 7(b) demonstrates the effect of coexisting ions such as Cl^-, SO_4^{2-}, and PO_4^{3-} on the removal of NO_3^- in individual binary mixtures of NO_3^-. Although ion exchange resins generally have a greater affinity towards ions with a higher atomic number and increasing valence,[71] Purolite SSTA63 anion exchange resin was presumed to have a still affinity for the NO_3^- ions than for the others, with a slight decrease in removal efficiency. >93% efficiency was recorded in the presence of other competing ions, suggesting a strong selectivity of the resin towards NO_3^-.

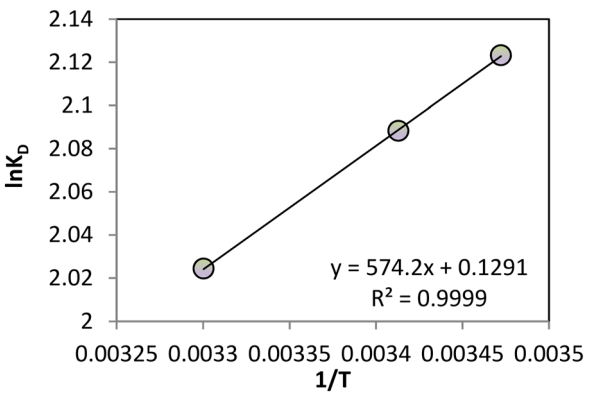

Fig. 6 $\ln K_D$ *vs.* $1/T$ plot for sorption thermodynamics of NO_3^- onto Purolite SSTA63 anion exchange resin.

3.7. Removal of NO_3^- from groundwater in an agricultural zone

After conducting comprehensive parametric tests with SSTA63 resin, the resin was applied to a real water sample obtained from the west side of Türkiye, Aydın. The composition of the water sample is detailed in Table 6.

25 mL of this water sample was mixed with 0.1 g of SSTA63 resin for 1 hour. After separation by decantation, the treated sample was analyzed for anion content using ion chromatography (IC). Following sorption, chloride concentration increased to 557.6 mg L^{-1}, sulfate

Table 5 Thermodynamic parameters for the sorption of NO_3^- onto Purolite SSTA63 anion exchange resin

Temperature (°C)	$\Delta G°$ (kJ mol^{-1})	$\Delta H°$ (kJ mol^{-1})	$\Delta S°$ (J mol^{-1} K^{-1})
15	−5.08	−4.77	+1.08
20	−5.09		
30	−5.10		

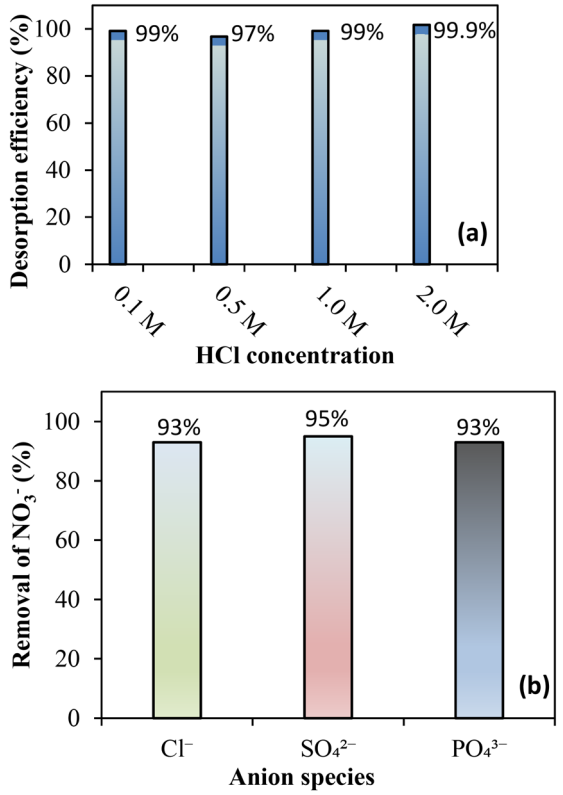

Fig. 7 (a) NO_3^- desorption efficiencies at different HCl concentrations, (b) the effect of coexisting anions on the removal efficiency of NO_3^-.

concentration decreased to 759.2 mg L^{-1}, and nitrate concentration decreased to 105.1 mg L^{-1}, achieving a 40% removal efficiency.

In the selectivity test, ion concentrations in the solution were adjusted to 100 mg L^{-1}, and the removal of NO_3^- was unaffected. However, in the real water sample, high concentrations of SO_4^{2-} and chloride inhibited the removal rate of NO_3^-. In a subsequent test, the resin dose in the solution was increased to 0.25 g, and 25 mL of water sample was treated with the resin. After 1 hour of shaking, the resin was removed, and the anion concentrations in the treated water were analyzed by IC. Results showed chloride concentration at 789.9 mg L^{-1}, NO_3^- at 62.3 mg L^{-1}, and SO_4^{2-} at 523.0 mg L^{-1}. Increasing the resin dose enhanced the removal rates of NO_3^- and SO_4^{2-}, achieving a 65% removal efficiency for NO_3^-.

Table 6 Composition of groundwater from the agricultural zone

Component	Value
Na^+ (mg L^{-1})	303.2
K^+ (mg L^{-1})	16.3
Ca^{2+} (mg L^{-1})	304.2
Mg^{2+} (mg L^{-1})	209.5
Cl^- (mg L^{-1})	315.0
SO_4^{2-} (mg L^{-1})	1017.8
NO_3^- (mg L^{-1})	176.5
pH	7.2
Conductivity (ms cm^{-1})	3.83

Despite high removal rates observed in aqueous solutions, the presence of interfering ions in the real water sample impacted the removal efficiency of NO_3^-.

3.8. Cost calculations for NO_3^- removal using SSTA63 resin

The resin price in Turkiye is 12 € per L. The resin capacity was determined to be 53.6 mg of NO_3^- per gram of resin. Additionally, 1 gram of dry resin is measured as 2.2 mL of wet volume. Therefore, the cost of treating 1 mg of NO_3^- amounts to 0.05 cents.

Conclusions

The investigation into Purolite Shallow Shell™ SSTA63 anion exchange resin's effectiveness in removing NO_3^- from aqueous solutions underscores its significant potential for water treatment. Optimum removal efficiency, surpassing 97%, was achieved at a resin dosage of 0.1 g and within pH levels ranging from 4 to 10. Analysis revealed an exothermic interaction between the resin and NO_3^- ions, complemented by efficient regeneration through desorption using hydrochloric acid, even at low concentrations of 0.1 M. Coexisting ions, such as Cl^-, SO_4^{2-}, and phosphate PO_4^{3-}, exerted minimal impact on NO_3^- removal, with efficiencies consistently exceeding 93%. These findings underscore the resin's robust performance in mitigating nitrate contamination in water sources and suggest avenues for further research aimed at practical application scaling. The results show that the resin performs optimally under specific conditions, providing a scalable and efficient solution for NO_3^- removal in water treatment processes. The findings have significant implications for the design of more sustainable and cost-effective water purification systems, particularly in regions facing high levels of NO_3^- contamination.

Data availability

Data will be available upon request.

Author contributions

Elif Çendik: funding acquisition, investigation. Mügenur Saygı: investigation. Yaşar Kemal Recepoğlu: writing – review & editing, conceptualization, visualization. Özgür Arar: writing – review &editing, supervision, resources, investigation.

Conflicts of interest

There are no conflicts to declare.

Acknowledgements

This study was supported by the Scientific and Technological Research Council of Türkiye (TUBITAK program code: 2209-A). We thank Purolite Int. Co. (Türkiye) for providing ion-exchange resin samples.

References

1 I. Ali, G. T. Imanova, H. M. Albishri, W. H. Alshitari, M. Locatelli, M. N. Siddiqui and A. M. Hameed, An ionic-liquid-imprinted nanocomposite adsorbent: Simulation, kinetics and thermodynamic studies of triclosan endocrine disturbing water contaminant removal, *Molecules*, 2022, **27**, 5358.

2 I. Ali, S. Z. Hasan, H. Garcia, M. K. Danquah and G. Imanova, Recent advances in graphene-based nano-membranes for desalination, *Chem. Eng. J.*, 2024, 149108.

3 I. Ali, G. T. Imanova, A. Alamri and S. Z. Hasan, Preparation of polyhydroquinone graphene oxide nanocomposite for cephalexin removal from water by adsorption: Simulation, kinetics, and thermodynamic studies, *Inorg. Chem. Commun.*, 2023, **157**, 111414.

4 J. Georgin, D. S. P. Franco, L. Meili, A. Bonilla-Petriciolet, T. A. Kurniawan, G. Imanova, E. Demir and I. Ali, Environmental remediation of the norfloxacin in water by adsorption: Advances, current status and prospects, *Adv. Colloid Interface Sci.*, 2024, 103096.

5 M. M. Urbano-Juan, M. M. Socías-Viciana and M. D. Ureña-Amate, Evaluation of nitrate controlled release systems based on (acrylamide-co-itaconic acid) hydrogels, *React. Funct. Polym.*, 2019, **141**, 82–90.

6 E. Craswell, Fertilizers and nitrate pollution of surface and ground water: an increasingly pervasive global problem, *SN Appl. Sci.*, 2021, **3**, 518.

7 M. H. Ward, R. R. Jones, J. D. Brender, T. M. De Kok, P. J. Weyer, B. T. Nolan, C. M. Villanueva and S. G. Van Breda, Drinking water nitrate and human health: an updated review, *Int. J. Environ. Res. Public Health*, 2018, **15**, 1557.

8 W. Laue, M. Thiemann, E. Scheibler and K. W. Wiegand, Nitrates and nitrites, *Ullmann's Encyclopedia of Industrial Chemistry*, 2000.

9 P. Santamaria, Nitrate in vegetables: toxicity, content, intake and EC regulation, *J. Sci. Food Agric.*, 2006, **86**, 10–17.

10 S. T. J. McDonagh, L. J. Wylie, C. Thompson, A. Vanhatalo and A. M. Jones, Potential benefits of dietary nitrate ingestion in healthy and clinical populations: A brief review, *Eur. J. Sport Sci.*, 2019, **19**, 15–29.

11 W. T. Clements, S.-R. Lee and R. J. Bloomer, Nitrate ingestion: a review of the health and physical performance effects, *Nutrients*, 2014, **6**, 5224–5264.

12 D. Xue, J. Botte, B. De Baets, F. Accoe, A. Nestler, P. Taylor, O. Van Cleemput, M. Berglund and P. Boeckx, Present limitations and future prospects of stable isotope methods for nitrate source identification in surface-and groundwater, *Water Res.*, 2009, **43**, 1159–1170.

13 W. H. O., *Guidelines for safe recreational water environments: Coastal and fresh waters*, World Health Organization, 2003, vol. 1.

14 M. Anas, F. Liao, K. K. Verma, M. A. Sarwar, A. Mahmood, Z.-L. Chen, Q. Li, X.-P. Zeng, Y. Liu and Y.-R. Li, Fate of nitrogen in agriculture and environment: agronomic, eco-physiological and molecular approaches to improve nitrogen use efficiency, *Biol. Res.*, 2020, **53**, 1–20.

15 M. Rashid, Q. Hussain, K. S. Khan, M. I. Alwabel, R. Hayat, M. Akmal, S. S. Ijaz and S. Alvi, Carbon-based slow-release fertilizers for efficient nutrient management: synthesis, applications, and future research needs, *J. Soil Sci. Plant Nutr.*, 2021, **21**, 1144–1169.

16 M. N. Khan, M. Mobin, Z. K. Abbas and S. A. Alamri, Fertilizers and their contaminants in soils, surface and groundwater, *Encyclopedia of the Anthropocene*, 2018, vol. 5, pp. 225–240.

17 M. Giordano, S. A. Petropoulos and Y. Rouphael, The fate of nitrogen from soil to plants: Influence of agricultural practices in modern agriculture, *Agriculture*, 2021, **11**, 944.

18 K. Javan, A. Altaee, S. BaniHashemi, M. Darestani, J. Zhou and G. Pignatta, A review of interconnected challenges in the water–energy–food nexus: Urban pollution perspective towards sustainable development, *Sci. Total Environ.*, 2023, 169319.

19 R. Dhanker, K. Khatana, K. Verma, A. Singh, R. Kumar and H. I. Mohamed, An integrated approach of algae-bacteria mediated treatment of industries generated wastewater: Optimal recycling of water and safe way of resource recovery, *Biocatal. Agric. Biotechnol.*, 2023, 102936.

20 R. Chauhan and V. C. Srivastava, A suitable combination of electrodes for simultaneous reduction of nitrates and oxidation of ammonium ions in an explosive industry wastewater, *Ind. Eng. Chem. Res.*, 2021, **60**, 5482–5493.

21 V. Babrauskas and D. Leggett, Thermal decomposition of ammonium nitrate, *Fire Mater.*, 2020, **44**, 250–268.

22 I. Oluwoye, B. Z. Dlugogorski, J. Gore, H. C. Oskierski and M. Altarawneh, Atmospheric emission of NOx from mining explosives: A critical review, *Atmos. Environ.*, 2017, **167**, 81–96.

23 J. E. Shelby, *Introduction to Glass Science and Technology*, Royal Society of Chemistry, 2020.

24 C. Villada, A. Bonk, T. Bauer and F. Bolívar, High-temperature stability of nitrate/nitrite molten salt mixtures under different atmospheres, *Appl. Energy*, 2018, **226**, 107–115.

25 I. Milton-Laskibar, J. A. Martínez and M. P. Portillo, Current knowledge on beetroot bioactive compounds: Role of nitrate and betalains in health and disease, *Foods*, 2021, **10**, 1314.

26 A. M. M. Attia, F. A. A. Ibrahim, N. A. Abd El-Latif, S. W. Aziz, A. M. Elwan, A. Aziz, A. Elgendy and F. T. Elgengehy, Role of reactive nitrogen species and antioxidant defense systems in the pathogenesis of rheumatoid arthritis, *Wulfenia*, 2015, **22**, 120–135.

27 P. K. Gupta and P. K. Gupta, Disposition and Fate of Toxicants, *Concepts and Applications in Veterinary Toxicology: An Interactive Guide*, 2019, pp. 27–44.

28 M. M. El-Dalatony and X. Li, Environmental Pollutants That Can Be Metabolized by the Host (Gut Microbiota), *Gut Remediation of Environmental Pollutants: Potential Roles of Probiotics and Gut Microbiota*, 2020, pp. 145–168.

29 K. R. Hakeem, M. Sabir, M. Ozturk, M. S. Akhtar and F. H. Ibrahim, Nitrate and nitrogen oxides: sources, health effects

and their remediation, *Reviews of Environmental Contamination and Toxicology*, 2017, vol. 242, pp. 183–217.
30 N. S. Bryan and H. van Grinsven, The role of nitrate in human health, *Adv. Agron.*, 2013, **119**, 153–182.
31 D. M. Manassaram, L. C. Backer, R. Messing, L. E. Fleming, B. Luke and C. P. Monteilh, Nitrates in drinking water and methemoglobin levels in pregnancy: a longitudinal study, *Environ. Health*, 2010, **9**, 1–12.
32 K. Said Abasse, E. E. Essien, M. Abbas, X. Yu, W. Xie, J. Sun, L. Akter and A. Cote, Association between dietary nitrate, nitrite intake, and site-specific cancer risk: a systematic review and meta-analysis, *Nutrients*, 2022, **14**, 666.
33 E. E. Essien, K. S. Abasse, A. Côté, K. S. Mohamed, M. M. F. A. Baig, M. Habib, M. Naveed, X. Yu, W. Xie and S. Jinfang, Drinking-water nitrate and cancer risk: A systematic review and meta-analysis, *Arch. Environ. Occup. Health*, 2022, **77**, 51–67.
34 W. Kruczkowska, M. Kciuk, Z. Pasieka, K. Kłosiński, E. Płuciennik, J. Elmer, K. Waszczykowska, D. Kołat and Ż. Kałuzińska-Kołat, The artificial oxygen carrier erythrocruorin —characteristics and potential significance in medicine, *J. Mol. Med.*, 2023, **101**, 961–972.
35 D. B. Kim-Shapiro, M. T. Gladwin, R. P. Patel and N. Hogg, The reaction between nitrite and hemoglobin: the role of nitrite in hemoglobin-mediated hypoxic vasodilation, *J. Inorg. Biochem.*, 2005, **99**, 237–246.
36 P. R. Gardner, Hemoglobin: a nitric-oxide dioxygenase, *Scientifica*, 2012, **2012**, 683729.
37 D. A. Nnate and N. K. Achi, Nitrate metabolism: a curse or blessing to humanity, *J. Sci. Res. Rep.*, 2016, **11**, 1–19.
38 R. A. F. Neves, S. M. Nascimento and L. N. Santos, Harmful algal blooms and shellfish in the marine environment: An overview of the main molluscan responses, toxin dynamics, and risks for human health, *Environ. Sci. Pollut. Res.*, 2021, **28**, 55846–55868.
39 J. Hradil, E. Králová and M. J. Beneš, Methacrylate anion exchangers with enhanced affinity for nitrates, *React. Funct. Polym.*, 1997, **33**, 263–273.
40 Y. Liu, X. Zhang and J. Wang, A critical review of various adsorbents for selective removal of nitrate from water: Structure, performance and mechanism, *Chemosphere*, 2022, **291**, 132728.
41 Y. Pang and J. Wang, Various electron donors for biological nitrate removal: A review, *Sci. Total Environ.*, 2021, **794**, 148699.
42 A. Santafé-Moros, J. M. Gozálvez-Zafrilla and J. Lora-García, Performance of commercial nanofiltration membranes in the removal of nitrate ions, *Desalination*, 2005, **185**, 281–287.
43 R. C. Scholes, M. A. Vega, J. O. Sharp and D. L. Sedlak, Nitrate removal from reverse osmosis concentrate in pilot-scale open-water unit process wetlands, *Environ. Sci.*, 2021, **7**, 650–661.
44 D. Xu, Y. Li, L. Yin, Y. Ji, J. Niu and Y. Yu, Electrochemical removal of nitrate in industrial wastewater, *Front. Environ. Sci. Eng.*, 2018, **12**, 1–14.
45 F. Ni, Y. Ma, J. Chen, W. Luo and J. Yang, Boron-iron nanochains for selective electrocatalytic reduction of nitrate, *Chin. Chem. Lett.*, 2021, **32**, 2073–2078.
46 M. Tang, Q. Tong, Y. Li, R. Jiang, L. Shi, F. Shen, Y. Wei, Z. Liu, S. Liu and J. Zhang, Effective and selective electrocatalytic nitrate reduction to ammonia on urchin-like and defect-enriched titanium oxide microparticles, *Chin. Chem. Lett.*, 2023, **34**, 108410.
47 S. Shyamala, N. A. Manikandan, K. Pakshirajan, V. T. Tang, E. R. Rene, H.-S. Park and S. K. Behera, Phytoremediation of nitrate contaminated water using ornamental plants, *J. Water Supply: Res. Technol.–AQUA*, 2019, **68**, 731–743.
48 T. Zhu, W. Cai, B. Wang, W. Liu, K. Feng, Y. Deng and A. Wang, Enhanced nitrate removal in an Fe 0-driven autotrophic denitrification system using hydrogen-rich water, *Environ. Sci.*, 2019, **5**, 1380–1388.
49 G. Al-Enezi, M. F. Hamoda and N. Fawzi, Ion exchange extraction of heavy metals from wastewater sludges, *J. Environ. Sci. Health, Part A: Toxic/Hazard. Subst. Environ. Eng.*, 2004, **39**, 455–464.
50 J. Van Deventer, Selected ion exchange applications in the hydrometallurgical industry, *Solvent Extr. Ion Exch.*, 2011, **29**, 695–718.
51 M. Berrios, J. A. Siles, M. A. Martín and A. Martín, Ion exchange, *Separation and Purification Technologies in Biorefineries*, 2013, pp. 149–165.
52 I. Ali, I. Burakova, E. Galunin, A. Burakov, E. Mkrtchyan, A. Melezhik, D. Kurnosov, A. Tkachev and V. Grachev, High-speed and high-capacity removal of methyl orange and malachite green in water using newly developed mesoporous carbon: kinetic and isotherm studies, *ACS Omega*, 2019, **4**, 19293–19306.
53 A. A. Basheer, Advances in the smart materials applications in the aerospace industries, *Aircr. Eng. Aerosp. Tech.*, 2020, **92**, 1027–1035.
54 Ö. Arar, Shallow Shell resin versus traditional resin: A case study for Cu (II) removal, *Anadolu Univ. J. Sci. Technol. A: Appl. Sci. Eng.*, 2016, **17**, 530–542.
55 A. Bhatnagar, E. Kumar and M. Sillanpää, Nitrate removal from water by nano-alumina: Characterization and sorption studies, *Chem. Eng. J.*, 2010, **163**, 317–323.
56 S. N. Milmile, J. V. Pande, S. Karmakar, A. Bansiwal, T. Chakrabarti and R. B. Biniwale, Equilibrium isotherm and kinetic modeling of the adsorption of nitrates by anion exchange Indion NSSR resin, *Desalination*, 2011, **276**, 38–44.
57 J. Yao, Z. Wang, M. Liu, B. Bai and C. Zhang, Nitrate-Nitrogen Adsorption Characteristics and Mechanisms of Various Garden Waste Biochars, *Materials*, 2023, **16**, 5726.
58 P. T. Phan, T. A. Nguyen, N. H. Nguyen and T. T. Nguyen, Modelling approach to nitrate adsorption on triamine-bearing activated rice husk ash, *Eng. Appl. Sci. Res.*, 2020, **47**, 190–197.
59 S. Samatya, N. Kabay, Ü. Yüksel, M. Arda and M. Yüksel, Removal of nitrate from aqueous solution by nitrate selective ion exchange resins, *React. Funct. Polym.*, 2006, **66**, 1206–1214.

60 M. Chabani, A. Amrane and A. Bensmaili, Kinetics of nitrates adsorption on Amberlite IRA 400 resin, *Desalination*, 2007, **206**, 560–567.
61 H. Song, Y. Zhou, A. Li and S. Mueller, Selective removal of nitrate from water by a macroporous strong basic anion exchange resin, *Desalination*, 2012, **296**, 53–60.
62 J. Ma, Z. Wang, Z. Wu, T. Wei and Y. Dong, Aqueous nitrate removal by D417 resin: thermodynamic, kinetic and response surface methodology studies, *Asia-Pac. J. Chem. Eng.*, 2012, **7**, 856–867.
63 X. Xu, B. Gao, Q. Yue, Q. Li and Y. Wang, Nitrate adsorption by multiple biomaterial based resins: Application of pilot-scale and lab-scale products, *Chem. Eng. J.*, 2013, **234**, 397–405.
64 X. Xu, B. Gao, Y. Zhao, S. Chen, X. Tan, Q. Yue, J. Lin and Y. Wang, Nitrate removal from aqueous solution by Arundo donax L. reed based anion exchange resin, *J. Hazard. Mater.*, 2012, **203**, 86–92.
65 M. Kalaruban, P. Loganathan, W. G. Shim, J. Kandasamy, G. Naidu, T. V. Nguyen and S. Vigneswaran, Removing nitrate from water using iron-modified Dowex 21K XLT ion exchange resin: Batch and fluidised-bed adsorption studies, *Sep. Purif. Technol.*, 2016, **158**, 62–70.
66 H. T. Banu and S. Meenakshi, Synthesis of a novel quaternized form of melamine–formaldehyde resin for the removal of nitrate from water, *J. Water Process Eng.*, 2017, **16**, 81–89.
67 Y. Sun and W. Zheng, Polyethylenimine-functionalized polyacrylonitrile anion exchange fiber as a novel adsorbent for rapid removal of nitrate from wastewater, *Chemosphere*, 2020, **258**, 127373.
68 Y. K. Recepoğlu, B. Arabacı, A. Kahvecioğlu and A. Yüksel, Granulation of Hydrometallurgically Synthesized Spinel Lithium Manganese Oxide Using Cross-Linked Chitosan for Lithium Adsorption from Water, *J. Chromatogr. A*, 2024, 464712.
69 I. Y. Ipek, Application of kinetic, isotherm, and thermodynamic models for atrazine adsorption on nanoporous polymeric adsorbents, *Sep. Sci. Technol.*, 2014, **49**, 2358–2365.
70 H. Nassar, A. Zyoud, A. El-Hamouz, R. Tanbour, N. Halayqa and H. S. Hilal, Aqueous nitrate ion adsorption/desorption by olive solid waste-based carbon activated using ZnCl2, *Sustainable Chem. Pharm.*, 2020, **18**, 100335.
71 A. Keränen, T. Leiviskä, O. Hormi and J. Tanskanen, Removal of nitrate by modified pine sawdust: Effects of temperature and co-existing anions, *J. Environ. Manage.*, 2015, **147**, 46–54.